Publications of the Astronomical Society of Japan, 2025, **00**, 1–7
doi: 10.1093/pasj/xxx000
Advance access publication date:

The unified rotation curve of the Galaxy sampled from the nucleus to halo: URC2026

Yoshiaki SOFUE[1]

[1]Institute of Astronomy, The University of Tokyo, 2-21-1 Mitaka, Tokyo 181-8588, Japan
*E-mail: sofue@ioa.s.u-tokyo.ac.jp

ORCID: 0000-0002-4268-6499

Abstract

We present the unified rotation curve (URC) of the Milky Way with the highest resolution and most complete sampling from the central super massive black hole (SMBH) to the outermost halo up to ~ 300 kpc. The URC consists of the following five mass components: 1. the fixed central SMBH, 2. massive core by exponential sphere with scale radius and mass of $(4\ \mathrm{pc},\ 4\times10^7 M_\odot)$, 3. bulge by exponential sphere $(150\ \mathrm{pc},\ 1.0\times10^{10} M_\odot)$, 4. exponential disk $(3.8\ \mathrm{kpc},\ 1.5\times10^{11} M_\odot)$, and 5. Navarro-Frenk-White halo with scale radius $h\sim14$ kpc and density $\rho_0\sim9\times10^{-3} M_\odot\ \mathrm{pc}^{-3}$, critical radius and mass with $R_{200}\sim81\ \mathrm{kpc}$ and $M_{200}^{\mathrm{total}}\sim4.2\times10^{11} M_\odot$. The lower limit to the local DM density at the Sun is estimated as ~0.24 GeV cm^{-3}($\sim6\times10^{-3} M_\odot\mathrm{pc}^{-3}$) as the value calculated for the NFW DH profile.

Keywords: galaxies: individual (Milky Way) — galaxies: rotation curve — Galaxy: kinematics and dynamics — galaxies: Cosmology – dark matter

1 Introduction

The rotation curve (RC) is the most fundamental tool for measuring the dynamical mass and its distribution in the Galaxy under the assumption that the galaxy is rotating around its polar axis (Sofue and Rubin 2001; Sofue 2017; Sofue 2020; Lelli et al. 2016; McGaugh 2016; Salucci 2019). In our earlier papers (Sofue et al. 2009; Sofue 2012; Sofue 2013) we have constructed a "unified RC (URC)" of the Galaxy from the nucleus to a half way to M31 including the outer halo by combining the existing rotation data in the decades from 1980's to 2000's. We have also deconvolved the URC into several mass components to obtain fundamental parameters such as the total mass and scale size of each component, as well as the local density of dark matter (DM) (Sofue 2013; Sofue 2020).

In this paper, we revise the URC of the Milky Way by employing the most recent data about Galactic rotation. We integrate the current RCs determined individually for the Galactic Center by the ALMA molecular line survey of the central molecular zone (CMZ) (Longmore et al. 2026; Sofue et al. 2025), the inner disk using the CO and HI-line surveys of the Galactic plane (Sofue & Kohno 2025), the stellar disk by trigonometry of maser sources using VERA (VERA Collaboration et al. 2020) and VLBA (Reid et al. 2019), the disk stars by GAIA trigonometry (Eilers et al. 2019), and 3D velocities of globular clusters and dwarf galaxies with GAIA (Jiao et al. 2023; Sylos Labini 2024). We adopt the Galactic constants $R_0=8.18\ \mathrm{kpc}$ (Gravity Collaboration et al. 2019) and $\Theta_0=235.1\ \mathrm{km\ s^{-1}}$ (Sofue & Kohno 2025).

We then use the URC to calculate the mass distribution in the Galaxy assuming circular motion, which is well confirmed by the 3D motion map by the VLBI trigonometry and proper motion observations (VERA Collaboration et al. 2020). There are two major methods to estimate the mass: (1) Dynamical (Virial-theorem) method and (2) photometry. The dynamical method uses kinematical data such as the rotation curve, and are widely used to measure the dynamical mass of the Galaxy and galaxies (Sofue and Rubin 2001; Sofue 2017; Sofue 2020). This method measures the total mass including black holes, stars, ISM, and dark matter, yielding the radial distribution of the mass density. However, it cannot discriminate the fraction of the individual species like DM from stars. Infrared photometry has been extensively performed of the nuclear stellar cluster, bulge and disk to measure the 3D distribution of red giant stars (Robin et al. 2012; Schödel et al. 2014; Portail et al. 2015; Wegg et al. 2015; Ness & Lang 2016; Valenti et al. 2016; Simion et al. 2017), which has given still spreading masses of the bulge and disk. In this paper, we perform the dynamical determination of the total mass distribution in the Galaxy, which will provide a basis to calibrate the photometry results.

2 Construction of URC26

2.1 Central black hole

The rotation curve around the central supermassive black hole (SMBH) located at the nucleus (Sgr A*) with a mass of $M_1=4.0\times10^6 M_\odot$ (Ghez et al. 2008; Gillessen et al. 2009) is represented by the Keplerian law.

2.2 Central Molecular Zone (CMZ)

We have recently determined the RC in the CMZ using the ACES survey data (Longmore et al. 2026) by applying the terminal velocity method to the longiutde-velocity diagrams (LVD) of the CS $(J=2-1)$-line emission from the molecular gas in the CMZ and the H40α-line from the ionized gas in the minispiral (Sofue et al. 2025). Figure 1 shows the RC inside $R\sim120$ pc. The entire CMZ

Received: , **Accepted:**

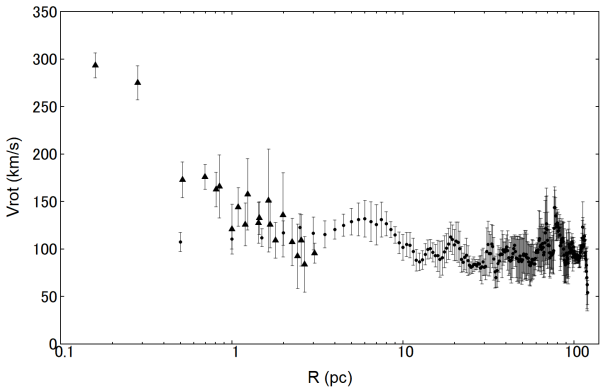

Fig. 1. Rotation curve of the CMZ in the central 120 pc obtained by terminal velocity method for H40α (triangles) and CS ($J=2-1$) (dots) lines in semilogarithmic scaling (Sofue et al. 2025). Alt text: Rotation curve of the Galactic Center.

has a nearly flat RC at $V_{\rm rot}\sim 100$ km s^{-1} associated with a peak around $R\sim 5$ pc. The innermost $V_{\rm rot}$ within $R\lesssim 1$ pc increases toward the nucleus, obeying the Keplerian law due to the central SMBH.

2.3 Gas disk by terminal velocities of CO and HI lines

Inside the solar circle ($-90^\circ \le l \le 90^\circ$), the rotation velocity $V(R)$ at the galacto-centric distance $R=R_0 \sin l$ is calculated simply by correcting the terminal velocity $V_{\rm term}$ for the circular motion of the LSR (local standard of rest) at the Sun:

$$V_{\rm rot}(R) = V_{\rm term} + \Theta_0 \sin l. \quad (1)$$

In figure 1 we show the inner RC obtained recently by Sofue & Kohno (2025), applying TVM to CO and HI line survey data of the Galactic plane (Dame et al. 2001; HI4PI Collaboration et al. 2016; Umemoto et al. 2017; Braiding et al. 2015; Cubuk et al. 2023).

2.4 Stellar disk by VLBI trigonometry of maser sources

Recent trigonometric measurements of maser sources using VERA (VLBI exploration of radio astrometry) (VERA Collaboration et al. 2020) and VLBA (very long baseline array) (Reid et al. 2019) have provided accurate 3D motions of the sources in the Galactic disk, which yielded circular rotational rotation curves at high accuracy. These results were combined with the inner RC from the terminal velocity to yield an RC from the Galactic Center to the halo at $R\sim 15$ kpc. In figure 2 we plot the circular velocities of maser sources from VERA by blue triangles and those by VLBA measurements by magenta dots.

2.5 Stellar disk and halo by GAIA trigonometry

The GAIA mission has provided proper motions of billions of stars in the Milky Way, and yielded high accuracy rotation curves of the mid to outer Galactic disk at $R\sim 8$ to 25 kpc (Eilers et al. 2019; Jiao et al. 2023; Sylos Labini 2024). We plot the circular velocities from GAIA DR3 by the inverse triangles in figure 2.

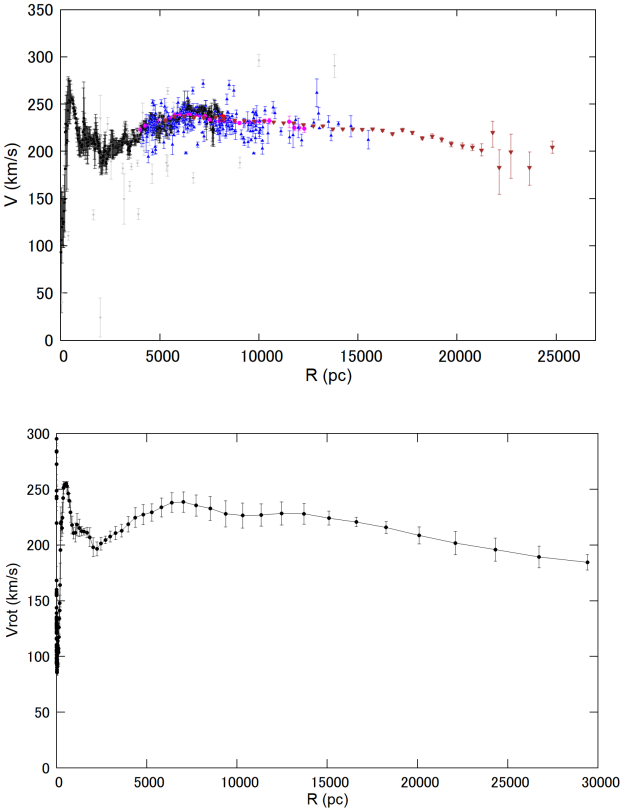

Fig. 2. RC up to 30 kpc by combining the inner RC of the gas disk using the terminal velocity method (black dots) (Sofue & Kohno 2025), trigonometry of maser sources with VERA (blue dots) (VERA Collaboration et al. 2020) and VLBA (magenta dots) (Reid et al. 2019), and disk stars by GAIA DR3 (brown triangles) (Jiao et al. 2023) by combining the RCs in figures 1 and 2. Alt text: URC26 added by $V_{\rm 3D}/\sqrt{2}$ of globular clusters and dwarf galaxies.

2.6 Halo RC from 25 to 100 kpc by globular clusters

For the outer Galactic halo, we employ GAIA trigonometric measurements of globular clusters (Vasiliev & Baumgardt 2021; Wang et al. 2022). In figure 3 we plot the circular rotation velocities presented by Wang et al. (2022), which cover $R\sim 25$ to ~ 100 kpc.

2.7 Halo RC from 25 to 300 kpc by dwarf galaxies

For ~ 25 to 300 kpc we use the 3D velocities observed by the GAIA trigonometry of dwarf galaxies (Li et al. 2017; Li et al. 2021; Hammer et al. 2021; Hammer et al. 2023). Following Sofue (2013) we introduce a "pseudo" rotation velocity of dwarf galaxies defined by

$$V_{\rm rot} = \eta V_{\rm 3D} = \eta \sqrt{v_{\rm RA}^2 + v_{\rm Dec}^2 + v_{\rm radial}^2}. \quad (2)$$

Here, v_i ($i=$RA, Dec, radial) are the velocities calculated for the proper motions and radial velocity with GAIA and η is a conversion factor of the 3D velocity to a pseudo circular velocity at the same radius. We assume $\eta\sim 1/\sqrt{2}$, considering that the dwarfs are half way to their apocenters and the orbital inclinations to the line of sights are random. We also examine a case with $\eta=1$, which will yield the upper limit of the circular velocity. Using the velocities thus converted we perform the Gaussian running average and plot them in figure 3. This "dwarf correction factor" η could vary

between $\eta \sim 1$ and $\sim 1/\sqrt{3}$, depending on the dynamical condition of the halo. This means that the dark halo mass estimation in this paper includes a systematic error of a factor of ~ 2.

2.8 URC26: Unified RC from the GC to outermost halo

We then construct a unified RC (URC) by taking the Gaussian running average (GRA) of the circular velocities $V(R_i)$ measured at $R = R_i$ for the i-th data points by the individual methods. The GRA value of V at a radius R is calculated by

$$V(R) = \Sigma_{i=1}^{N} V_i w_i \ / \ \Sigma_{i=1}^{N} w_i \tag{3}$$

and

$$\delta V = \left[\Sigma (V(R) - V_i)^2 w_i \ / \ \Sigma w_i\right]^{1/2}, \tag{4}$$

where

$$w_i = \exp\left[-(R_i - R)^2 \ / \ \delta R^2\right] \sigma_i^{-2}, \tag{5}$$

and σ_i is the error of the observed value of the i-th data point and $\delta R \sim 0.1R$ is the smoothing width. We plotted the URC in figure 3 at the same logarithmic radius interval.

Figure 4 shows a simultaneous plot of the RC that includes the SMBH, CMZ, bulge, disk, halo, and outer halo up to ~ 300 kpc, about half way to the Andromeda galaxy, in logarithmic scaling. We name this diagram the "URC26" (unified rotation curve 2026).

3 Discussion

3.1 Basic methods to derive the dynamical mass

We use the dynamical method based on the Virial theorem, which is a direct method using kinematical data such as the rotation curve. Widely adopted models to represent the bulge and disk are exponential sphere, exponential disk, Sérsic type potential, Miyamoto-Nagai potential, and the Plummer potential. We here adopt the exponential sphere for the core and bulge, and a flat exponential disk for the disk component. We comment that all these models yield rotation curves similar to each other composed of a rigid-body rise, a peak at ~ 2 scale radiii, and a Keplerian decrease, coinciding within a few percent with each other.The good agreement for different models is due to the long range of the gravitational force and the fast decrease in the density outside the scale radius in these models. However, NFW type potentials for the halo behaves quite differently, diverging outward because of the slow decrease of density.

3.2 Deconvolution of URC26 into dynamical mass components

The rotation curve is represented by a superposition of N dynamical mass components as

$$V_{\rm rot}(R) = \sqrt{\Sigma_{i=1}^{N} V_i(R)^2}, \tag{6}$$

where $V_i(R)$ is the circular velocity at radius R due to the i-th component. By a close look into URC26 in figure 4 we recognize five ($N = 5$) distinct mass components characterized by five velocity peaks at the center ($R \sim 0$ pc), $R \sim 5$ pc, ~ 500 pc, ~ 5000 pc and an outskirt that extends to $R \sim 300$ kpc. We here attribute these peaks to 1) SMBH, 2) core, 3) bulge, 4) disk, and 5) dark halo, and try to fit URC26 by superposition of these mass components by employing the following profiles. We then decompose the observed RC into the five components by the least-χ^2 method using the following functions representing the individual components. The fitted parameters are listed in table 1

3.2.1 Supermassive black hole

The innermost rotation curve at $R \lesssim 1$ pc is represented by the Keplerian law for the massive black hole with $M_{\rm BH} = 4 \times 10^6 M_\odot$ (Ghez et al. 2008; Gillessen et al. 2009):

$$\phi = GM_1/R, \tag{7}$$

and

$$V(R) = V_1/\sqrt{R/a_1} \tag{8}$$

with $V_1 = 131.5$ km s^{-1}and $a_1 = 1$ pc.

3.2.2 Core and bulge by exponential spheres

The disk to mid-halo RC at ~ 1 to ~ 15 kpc can be fitted by three components of a core, bulge, and disk. We adopt exponential density profile expressed as

$$\rho_i(R) = \rho_0^i \exp(-R/a_i), \tag{9}$$

where ρ_0^i and a_i are the central density and scale radius of the i-th mass component. The rotation velocity is calculated by

$$V_{{\rm rot}\,i}(R) = \sqrt{GM_i(R)/R}, \tag{10}$$

where

$$M_i(R) = \int_0^R \rho_i(r) 4\pi r^2 dr \tag{11}$$

is the enclosed mass inside R. We stress that because gravity has a long range force, the Plummer potential is a good approximation to that of an exponential density distribution, and any similar mass concentrations with sufficiently rapid density decrease, in an accuracy of a few percent (Sofue 2017).

By fitting to URC we obtain the scale radius and mass for the bulge to be $a_2 \simeq 2.4$ pc and $M_2 \simeq 3.3 \times 10^7 M_\odot$, and for bulge $a_3 \simeq 163$ pc and $M_3 \simeq 1.10 \times 10^{10} M_\odot$.

3.2.3 Exponential disk

The galactic disk is generally represented by an exponential disk (Freeman 1970), where the surface mass density (SMD) is expressed as

$$\Sigma_{\rm d}(R) = \Sigma_0 \exp(-R/a_{\rm d}). \tag{12}$$

Here, $\Sigma_{\rm d}$ is the central value, R_d is the scale radius. The total mass of the exponential disk is given by $M_{\rm disk} = 2\pi\Sigma_0 a_{\rm d}^2$. The circular velocity is expressed by

$$V_{\rm d}(R) = V_0 \sqrt{y^2[I_0(y)K_0(y) - I_1(y)K_1(y)]}, \tag{13}$$

where

$$V_0 = \sqrt{4\pi G \Sigma_0 a_{\rm d}} = \sqrt{2GM_{\rm disk}/a_{\rm d}} \tag{14}$$

or

$$M_{\rm disk} = \frac{1}{2}\frac{a_{\rm d} V_0^2}{G}, \tag{15}$$

with $y = R/(2a_{\rm d})$, and I_i and K_i are the modified Bessel functions.

By fitting we obtain the disk radius and mass of $a_4 \simeq 3.8$ kpc and $M_4 \simeq 1.6 \times 10^{11} M_\odot$.

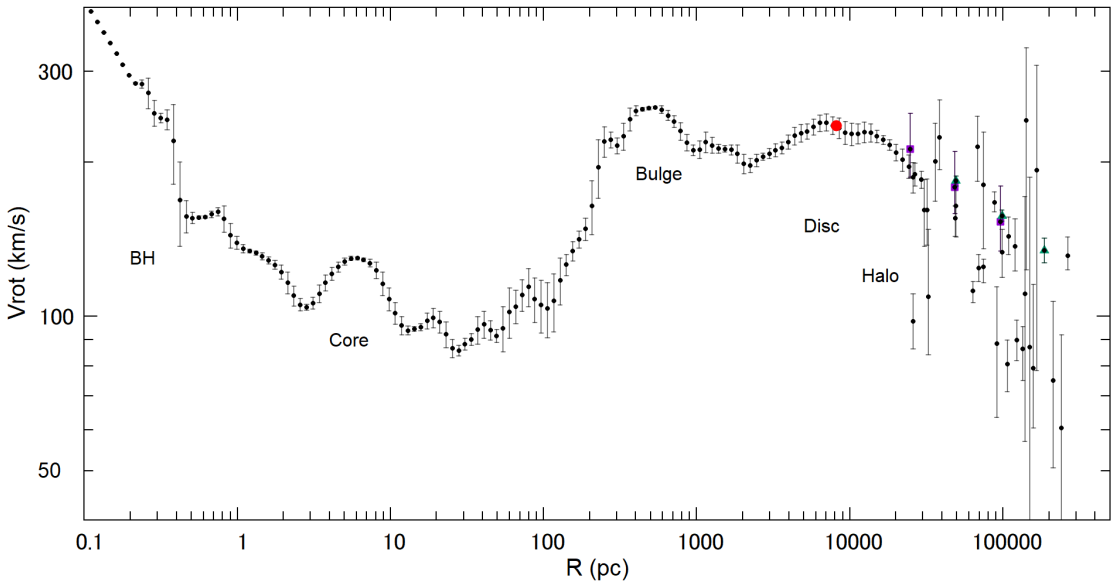

Fig. 3. The unified rotation curve URC2026 from figures 1 and 2 with GAIA trigonometric rotation curves of globular clusters from $R \gtrsim 25$ to 100 kpc by blue triangles and diamonds (Eadie & Jurić 2019; Vasiliev & Baumgardt 2021; Wang et al. 2022) and dwarf galaxies for $\eta = 1/\sqrt{2}$ by black dots (Li et al. 2021; Hammer et al. 2021; Hammer et al. 2023). Grey dots are disk RC from figure 2. The innermost Keplerian curve represents the SMBH of $4 \times 10^6 M_\odot$ (Ghez et al. 2008). We recognize five major components (velocity maxima) which can be attributed to the SMBH (component 1), core (component 2), bulge (3), and disk (4) and the dark halo (5). The big dot marks the Sun at $(8.2\ \mathrm{kpc},\ 235\ \mathrm{km\ s^{-1}})$. Alt text: Unified rotation curve from the GC to halo.

3.2.4 Dark halo by NFW profile

The extended outskirts of the URC beyond $R \sim 15$ kpc can be fitted by the dark halo represented by the NFW density profile (Navarro et al. 1997),

$$\rho_5(x) = \frac{\rho_0}{x(1+x)^2}, \tag{16}$$

where $x = R/h$ and $h = a_5$ is the scale radius. The rotation velocity is given by

$$V_{\mathrm{rot}5}(R) = \sqrt{GM_5(R)/R}, \tag{17}$$

and the mass inside R is given by

$$M_5(R) = 4\pi\rho_0 h^3[\ln(1+x) - x/(1+x)]. \tag{18}$$

By fitting we obtain $h \sim 13.6$ kpc and $\rho_0 = 8.8 \times 10^{-3} M_\odot$ pc^{-3}. Combining these values with those obtained for the bulge and disk and referring to URC26, as shown in figure 5, we obtain the critical radius and mass of the Galaxy to be $R_{200} \sim 80$ kpc at which the mass density becomes equal to the cosmological critical density, $\rho_{200} = 200 \times (3H_0^2)/(8\pi G) = 1.9 \times 10^{-27}$g cm^{-3} = $2.8 \times 10^{-5} M_\odot$pc^{-3} with $H_0 = 71$ km s^{-1}Mpc^{-1} being the Hubble constant. The critical mass is obtained as $M_{200} = M(R_{200}) \sim 4 \times 10^{11} M_\odot$.

3.2.5 Mass and density distributions

The least χ^2 fitting results using these functions are summarized in table 1. The circular velocity was calculated using the fitted parameters and plotted in Figure 4. The calculated RC reproduces URC26 from the center to R 30 kpc well, and the outer halo (up to 300 kpc) also shows a reasonable fit within the margin of error. URC26 demonstrates the existence of a massive halo in the outermost region up to $R \sim 300$ kpc, which can be reasonably represented by the NFW mass model. However, URC26 does not support the Keplerian decrease in rotation velocity at $R \gtrsim 25$ kpc.

Table 1. Fitting parameters of the URC26 for $\eta = 1/\sqrt{2}$.

i-th component	Parameter
1. SMBH	$M_1 \simeq 4.0 \times 10^6 M_\odot$ ‡
2. Core	$a_2 \simeq 2.44 \pm 0.03$ pc
	$M_2 \simeq (3.33 \pm 0.06) \times 10^7 M_\odot$
3. Bulge	$a_3 \simeq 162 \pm 1.3$ pc
	$M_3 \simeq (1.12 \pm 0.01) \times 10^{10} M_\odot$
4. Disk	$a_4 \simeq 3.82 \pm 0.06$ kpc
	$M_4 \simeq (1.66 \pm 0.04) \times 10^{11} M_\odot$
5. Dark halo	$4\pi\rho_0 h^3 \sim (2.78 \pm 0.08) \times 10^{11} M_\odot$
	$\rho_0 = (8.82 \pm 0.25) \times 10^{-3} M_\odot \mathrm{pc}^{-3}$
	$a_5 = h \simeq 13.6 \pm 0.5$ pc
	$R_{200} \sim 81$ kpc
	$M_{200} \sim 4.2 \times 10^{11} M_\odot$

‡ Ghez et al. (2008)

Using dynamically fitted parameters, the density distribution and cumulative mass were calculated as a function of R and plotted in Figure 5. This diagram shows that mass is concentrated at a high density over a range of more than 10 orders of magnitude, from the dark halo to the nucleus.

The local density of DM is a key parameter for the direct detection experiments of DM. Using figure 5 (equation 16) we obtain the local density of DM at the Sun due to the dark halo alone to be $\rho_\odot^{\mathrm{DM}} \sim 6.2 \times 10^{-3} M_\odot \mathrm{pc}^{-3} \simeq 0.24$ GeV cm^{-3} . Note that this value represents only the dark halo contribution, not including the DM in the disk and bulge. So, this is a lower limit of the DM density near the Sun.

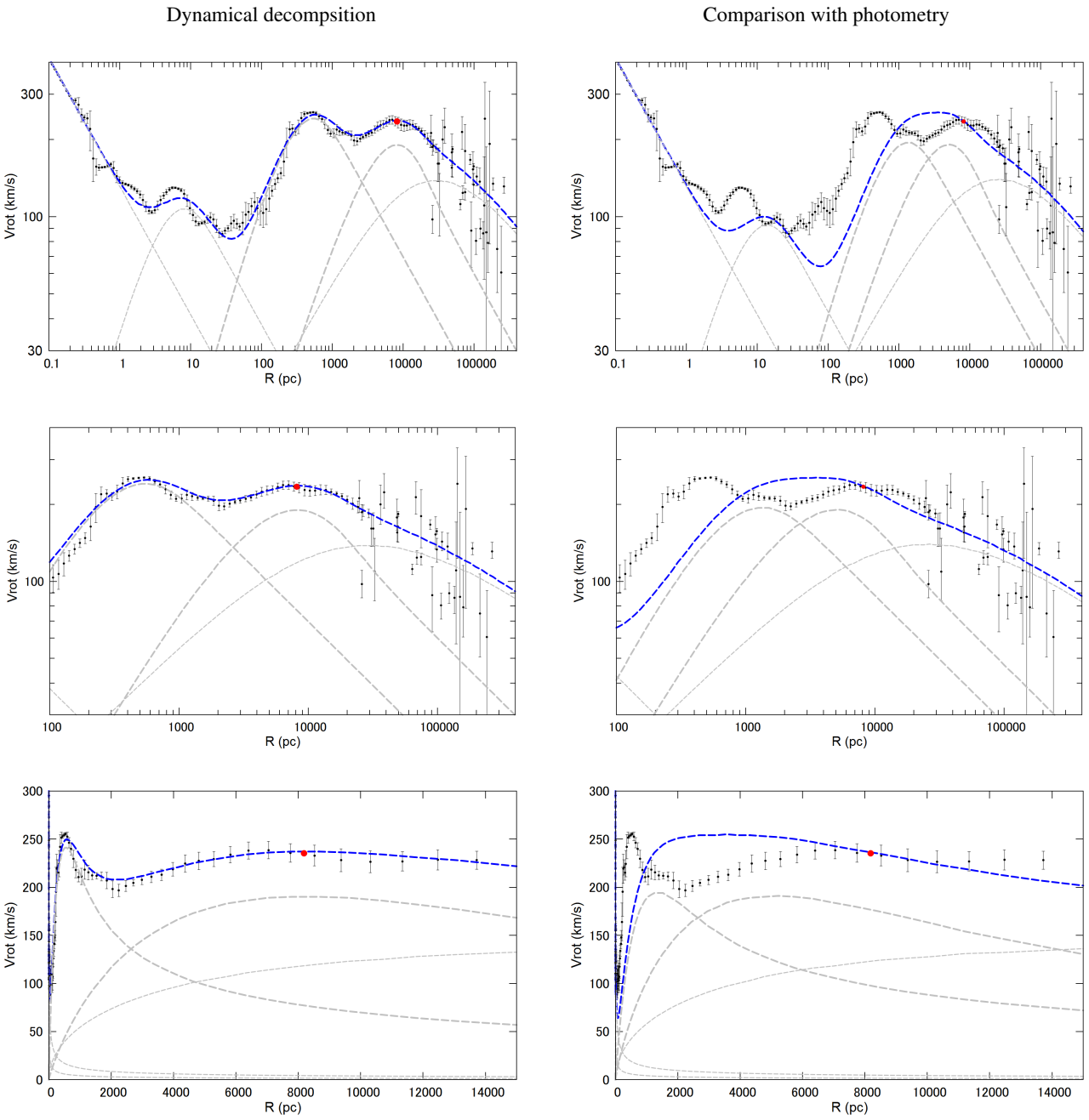

Fig. 4. χ^2 fitting result of URC26 by five dynamical mass components for parameters given in table 1 (left panels) compared with a rotation curve calculated for the photometry values for the core, bulge and disk (right panels). [Top] Logarithmic plot from the nucleus to outer halo. [Middle] Close up from the disk to halo. [Bottom] Close up of the inner Milky Way in linear scaling. Alt text: URC26 compared with that calculated for photometric results and possible fitting by 5 dynamical components.

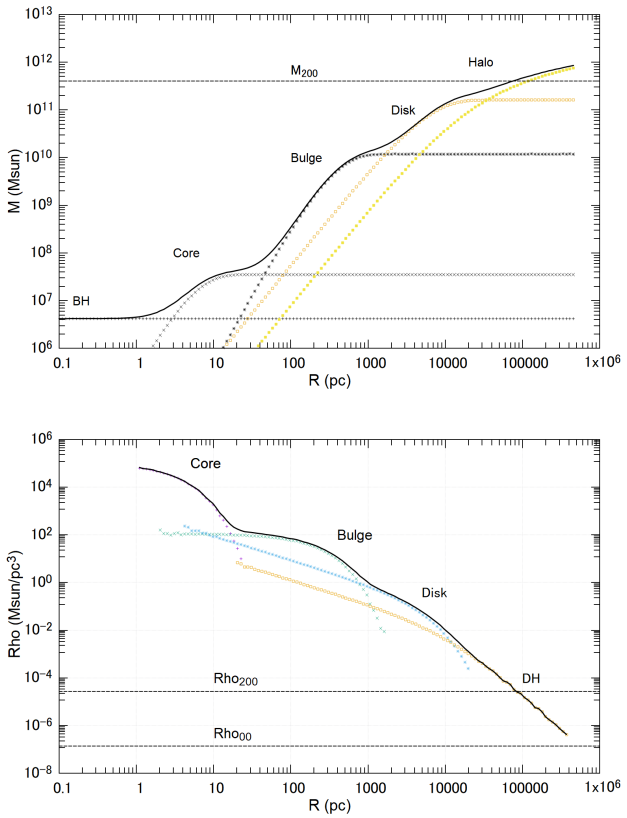

Fig. 5. [Top] Cumulative mass $M(R)$ calculated for the observed values of rotation velocity $\eta = 1/\sqrt{2}$ (dots) and least-χ^2 fitted URC using Plummer potential for the core, bulge and disk (thin line). Magenta triangles show the mass calculated for $\eta = 1$ (open triangles). [Bottom] Volume density calculated for the fitted URC in the top panel. Alt text: Cumulative mass and density distributions.

3.3 Comparison with the results by photometry

Extensive photometric observations in infrared wavelengths at ~ 2 to $\sim 4\mu$m have been obtained of the central stellar disk (Schödel et al. 2014), the bulge and disk (Robin et al. 2012; Robin et al. 2014; Wegg et al. 2015; Portail et al. 2015; Ness & Lang 2016; Valenti et al. 2016; Simion et al. 2017; Marasco et al. 2025). We here calculate circular velocities using the parameters obtained by photometry, and compare with the observed URC26 and the dynamical fitting result. For the SMBH and dark halo, we use the results from the previous subsections.

3.3.1 Photometric core (nuclear stellar disk)

We adopt the photometric scale radius and mass of the central stellar cluster, $a_2 \simeq 4.1$ pc and $M_2 \sim 4.2 \times 10^7 M_\odot$, from the infrared photometry by Schödel et al. (2014). These values are close to the dynamical values in table 1, and the resulting circular velocity is consistent with the dynamical RC in figure 4.

3.3.2 Photometric bulge

There have been extensive photometric measurements of the scale radius and luminous mass of the Galactic bulge. As median values of the current photometric measurements (Robin et al. 2012; Robin et al. 2014; Wegg et al. 2015; Portail et al. 2015; Ness & Lang 2016; Valenti et al. 2016; Simion et al. 2017), we provisionally adopt a scale radius of $a_3 \sim 400$ pc corresponding to the minor axis radius of the barred bulge and mass of $M_3 \sim 1.8 \times 10^{10} M_\odot$. The amplitude of the calculated circular velocity for the photometric parameters agrees with the observation, while the maximum velocity radius is largely displaced from that of the URC26 by about three times corresponding to the ratio of the photometric to dynamical radii of ~ 400 pc and ~ 150 pc. This causes the too mild rise of of the photometric rotation curve to fit the observed steep rise.

Several reasons are considered for the disagreement between the photometric and dynamical RCs of the bulge.

- Photometry might miss a higher concentration near the Galactic plane because the analyses are done avoiding the highly obscured belt in the Galactic plane at $|b| \lesssim 2\,\mathrm{deg}$.
- The conversion from surface brightness from photometry [Jy str^{-1} to dynamical mass [g cm^{-2}] might miss some spatial effect.
- The observed radial velocity used in the URC might represent non-circular motion due to eccentric orbits in the barred potential as indicated by photometry. However, this requires for the eccentric motion to occur far inside the photometric bulge, which is dynamically difficult. Also, no high eccentric motion is observed in the 3D motion of maser sources in the region under discussion (VERA Collaboration et al. 2020).

Therefore, the large difference of the photometric and dynamical RCs of the inner Milky Way remains a mystery.

3.3.3 Photometric disk

We adopt a scale radius of $a_4 \simeq 2.4$ kpc according to the surface photometry by Robin et al. (2014); Simion et al. (2017), and adjust the total mass to $M_4 \simeq 1.5 \times 10^{11} M_\odot$ so that the rotation velocity at the Sun matches the local value of $V_0 = 235$ km s^{-1}. The calculated RC well agrees with the dynamical RC fitted in the previous sections, and the parameters are close to each other. Although the dynamical scale radius of 3.8 kpc is slightly greater than the photometry value of 2.4 kpc, difference would be within an allowable range of uncertainty considering the photometry measures only the luminous stars not sensitive to gas and dark matter coexisting in the disk.

3.4 Scaling relation

The deconvolution of the RC into the components enables us to examine the scaling relation between the scale radius, a_i, and total mass, M_i, of the five mass components of the BH, core, bulge, disk and dark halo. For the BH, we define the scale radius as the radius at which the gravity of the BH dominates that of the core component, i.e., $a_{\rm BH} \sim 0.5$ pc. Figure 6 shows the total masses thus derived against the scale radii of the five components. We find a linear proportionality between the radius and the total mass, which varies by more than six orders of magnitude, and is expressed by $M \sim 10^7 M_\odot (R/1\ \mathrm{pc})^{1.1}$, as shown by the straight line in the figure. The diagram may provide a scaling relation within an individual galaxy about the coevolution of the BH, bulge, disk, and dark halo. This provides a complementary relation to the scaling law between the masses of the BHs and bulges among different galaxies (Kormendy & Ho 2013).

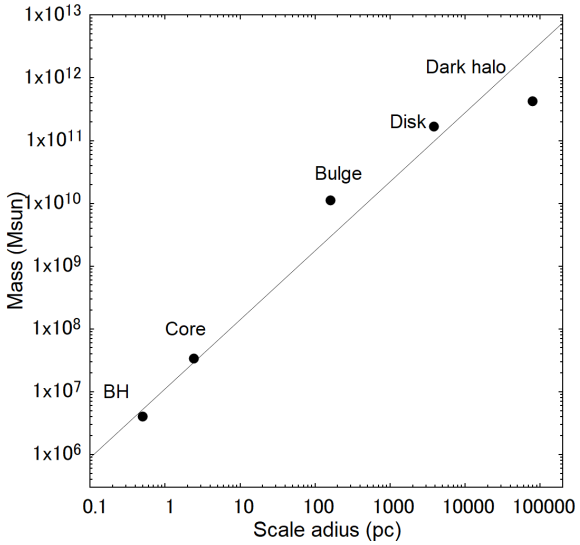

Fig. 6. Scale radius vs total mass of the five mass components of the Milky Way. The radius for BH is approximated by its 'gravity dominant radius'. The upper and lower dots for the DH represent M_{200} (including bulge and disk) and $M_{200}^{\rm DM}$ (DH component alone), respectively. The straight line indicates $M = 10^7 (R/1{\rm pc})^{1.1} M_\odot$. Alt text: Scaling relation among the deconvolved mass components.

4 Summary

We derived the most completely sampled unified rotation curve of the Milky Way (URC26) from the central super massive black hole to the outer halo of radius ~ 300 kpc, which has the highest resolution and accuracy ever performed. The URC was decomposed into five dynamical components of the central black hole with a mass of $M_1 = 4 \times 10^6 M_\odot$, the core with $M_2 \simeq 3.3 \times 10^7 M_\odot$ (core), the bulge with $M_3 \simeq 1.1 \times 10^{10} M_\odot$ (bulge), disk with $M_4 \simeq 1.6 \times 10^{11} M_\odot$ (disk), and the dark halo with the critical mass of $M_{200} \sim 4.2 \times 10^{11} M_\odot$ in the critical radius $R_{200} \sim 81$ kpc. The local dark matter density near the Sun due to the dark halo alone is estimated to be $\rho_\odot^{\rm DM} \sim 0.24$ GeV cm^{-3} . We found a linear proportionality between the scale radius and the mass of individual components.

Acknowledgments

Data analysis was performed at the NAOJ Astronomy Data Center.

Conflict of interests

The author declares that there are no conflicts of interest.

Data availability

The rotation curve used in this paper is downloadable from the PASJ supplementary cite at "http: (to be given by PASJ)" .

References

Braiding, C., Burton, M. G., Blackwell, R., et al. 2015, PASA, 32, e020.
Cubuk, K. O., Burton, M. G., Braiding, C., et al. 2023, PASA, 40, e047.
Dame, T. M., Hartmann, D., & Thaddeus, P. 2001, ApJ, 547, 2, 792.
Eadie, G. & Jurić, M. 2019, ApJ, 875, 2, 159.
Eilers, A.-C., Hogg, D. W., Rix, H.-W., et al. 2019, ApJ, 871, 1, 120.
Freeman, K.C. On the Disks of Spiral and S0 Galaxies. Astrophys. J. 1970, 160, 811.
Ghez, A.M.; Salim, S.; Weinberg, N.N.; et al.ApJ 2008, 689, 1044.
Gillessen, S.; Eisenhauer, F.; Trippe, S.; Alexander, T.; Genzel, R.; Martins, F.; Ott, T. ApJ 2009, 692, 1075.
Ginsburg, A., et al. submitted to MNRAS.
Gravity Collaboration, Abuter, R., Amorim, A., et al. 2019, A&A, 625, L10.
Hammer, F., Wang, J., Pawlowski, M. S., et al. 2021, ApJ, 922, 2, 93.
Hammer, F., Li, H., Mamon, G. A., et al. 2023, MNRAS, 519, 4, 5059.
HI4PI Collaboration, Ben Bekhti, N., Flöer, L., et al. 2016, A&A, 594, A116.
Jiao, Y., Hammer, F., Wang, H., et al. 2023, A&A, 678, A208.
Kormendy, J. & Ho, L. C. 2013, ARA&A, 51, 1, 511. doi:10.1146/annurev-astro-082708-101811
Lelli, F., McGaugh, S. S., & Schombert, J. M. 2016, AJ, 152, 6, 157. doi:10.3847/0004-6256/152/6/157
Li, Z.-Z.; Jing, Y.P.; Qian, Y.-Z.; Yuan, Z.; Zhao, D.-H. ApJ 2017, 850, 116.
Li, H., Hammer, F., Babusiaux, C., et al. 2021, ApJ, 916, 1, 8.
Longmore, S. N., Bally, J., Barnes, A. T., et al. 2026, arXiv:2602.20340. doi:10.48550/arXiv.2602.20340
McGaugh, S. S. 2016, ApJ, 816, 1, 42.
Marasco, A., Fall, S. M., Di Teodoro, E. M., et al. 2025, A&A, 695, L23. doi:10.1051/0004-6361/202553925
Miyamoto, M. & Nagai, R. 1975, PASJ, 27, 533.
Navarro, J.F.; Frenk, C.S.; White, S.D.M.ApJ. 1997, 490, 493.
Ness, M. & Lang, D. 2016, AJ, 152, 1, 14. doi:10.3847/0004-6256/152/1/14
Poggiani, R. 2025, Galaxies, 13, 3, 65.
Portail, M., Wegg, C., Gerhard, O., et al. 2015, MNRAS, 448, 1, 713.
Reid, M. J., Menten, K. M., Brunthaler, A., et al. 2019, ApJ, 885, 2, 131.
Robin, A. C., Marshall, D. J., Schultheis, M., et al. 2012, A&A, 538, A106.
Robin, A. C., Reylé, C., Fliri, J., et al. 2014, A&A, 569, A13.
Salucci, P.A&Ap. Rev. 2019, 27, 2.
Schödel, R., Feldmeier, A., Kunneriath, D., et al. 2014, A&A, 566, A47. doi:10.1051/0004-6361/201423481
Simion, I. T., Belokurov, V., Irwin, M., et al. 2017, MNRAS, 471, 4, 4323.
Söding, L., Bartel, R. L., & Mertsch, P. 2025, MNRAS, 542, 4, 2987.
Sofue, Y. 2012, PASJ, 64, 75.
Sofue, Y. PASJ 2013, 65, 118.
Sofue, Y.PASJ 2017, 69, R1.
Sofue, Y.; Rubin, V.ARA&Ap 2001, 39, 137.
Sofue, Y. 2020, Galaxies, 8, 37.
Sofue, Y.; Honma, M.; Omodaka, T. PASJ 2009, 61, 227.
Sofue, Y. & Kohno, M. 2025, PASJ, 77, 6, 1335.
Sofue, Y., Oka, T., Longmore, S. N., et al. 2025, arXiv:2504.03331.
Sylos Labini, F. 2024, ApJ, 976, 2, 185.
Umemoto, T., Minamidani, T., Kuno, N., et al. 2017, PASJ, 69, 78
Valenti, E., Zoccali, M., Gonzalez, O. A., et al. 2016, A&A, 587, L6.
VERA Collaboration, Hirota, T., Nagayama, T., et al. 2020, PASJ, 72, 4, 50.
Walker, D. L., et al. 2025, submitted to MNRAS
Wegg, C., Gerhard, O., & Portail, M. 2015, MNRAS, 450, 4, 4050.
Vasiliev, E. & Baumgardt, H. 2021, MNRAS, 505, 4, 5978.
Wang, J., Hammer, F., & Yang, Y. 2022, MNRAS, 510, 2, 2242.
White, M. 2001, A&A, 367, 27.